RSC Advances

PAPER

View Article Online
View Journal | View Issue

Cite this: *RSC Adv.*, 2023, **13**, 30633

Advancing structural batteries: cost-efficient high-performance carbon fiber-coated $LiFePO_4$ cathodes†

Jaehoon Choi, Omid Zabihi, Mojtaba Ahmadi and Minoo Naebe *

Structural batteries (SBs) have gained attention due to their ability to provide energy storage and structural support in vehicles and airplanes, using carbon fibers (CFs) as their main component. However, the development of high-performance carbon fiber-based cathode materials for structural batteries is currently limited. To address this issue, this study proposes a cost-efficient and straightforward method for creating a high-performance structural lithium iron phosphate ($LiFePO_4$) positive electrode by coating carbon fibers at mild temperatures and pressures. The resulting cathode demonstrated a high $LiFePO_4$ loading (at least 74%) and a smooth coating, as confirmed by X-ray spectroscopy, scanning electron microscopy, and Raman spectroscopy. This structural cathode exhibited a capacity of 144 mA h g^{-1} and 108 mA h g^{-1} at 0.1 C and 1.0 C, respectively. Additionally, the $LiFePO_4$ cathode displayed excellent electrochemical properties, with a capacity retention of 96.4% at 0.33 C and 81.2% at 1.0 C after 300 cycles. Overall, this study presents a promising approach for fabricating high-performance structural batteries with enhanced energy storage and structural capabilities.

Received 2nd August 2023
Accepted 4th October 2023

DOI: 10.1039/d3ra05228a

rsc.li/rsc-advances

Introduction

The demand for eco-friendly transportation has been on the rise worldwide, partly driven by carbon-neutral regulations set to take effect by 2050. Consequently, electric vehicles (EVs) have garnered increasing interest from investors in research and development as well as commercialization.[1,2] Lithium-ion batteries (LiBs) are widely investigated for use in EVs. However, one of the key challenges faced by EVs is their relatively shorter range per charging cycle, when compared to combustion engine vehicles. Therefore many studies are currently focused on enhancing the energy density of LiBs to address this limitation and make EVs more practical for daily use.[3–5]

Carbon fibers (CFs) are being utilized as a replacement for heavy car panels due to their lightweight and strong characteristics. This makes them an ideal material for improving energy efficiency by reducing the weight of vehicles.[6–8] Additionally, the graphitic structure of CFs allow energy storage[9,10] and its outstanding electrical conductivity makes it ideal to be used as a current collector.[11,12] Due to these unique characteristics CFs have been investigated to realize structural batteries which enables not only carrying mechanical load, but also simultaneously storing energies.[13,14] A structural composite battery is made up of carbon fibres that act as a reinforcing structure, electrode, and solid polymeric electrolyte which serves as both a separator and an electrolyte.[13,15–17]

At the early stage of research for structural batteries, there were significant focuses on developing CFs based anode as well as efforts to integrate CFs to fabricate CFs-composite electrode *via* solid polymer electrolyte.[18,19] However, there have not been many research on development of positive electrodes for structural batteries. To fabricate a positive electrode for structural batteries, there are various cathode materials such as $LiCoO_2$, $LiMn_2O_4$, $LiFePO_4$, which can be used in the conventional LiBs due to not only its considerable theoretical capacity (170 mA h g^{-1}) but also structural stability.[20–22]

Liu *et al.* reported carbon nanofiber based lithium cobalt oxide ($LiCoO_2$) cathode holding a specific capacity of 90 mA h g^{-1}.[19] However, carbon nanofiber is not only being used more commonly as an additive rather than a current collector, but also requires a slow dry casting process to remove the plasticizer (propylene carbonate). Recently, coating cathode material onto CFs *via* electrophoretic deposition (EPD) and autoclave method have been investigated for use in structural batteries.[11,23,24] Hagberg *et al.* reported that $LiFePO_4$ coated onto polyacrylonitrile (PAN)-based CFs tow *via* EPD method delivers a specific capacity of 108 mA h g^{-1} at 0.1 C.[11] However, the coating performance was dependent on the distance between Pt wire (counter electrode) and CFs (working electrode) at EPD instrumental set-up, making it difficult to obtain a high yield.

Carbon Nexus, Institute for Frontier Materials (IFM), Deakin University, Waurn Ponds, VIC, 3216, Australia. E-mail: minoo.naebe@deakin.edu.au

† Electronic supplementary information (ESI) available. See DOI: https://doi.org/10.1039/d3ra05228a

Park *et al.* reported a method using vacuum bag and autoclave to coat $LiFePO_4$ onto woven carbon fibre, and recorded a capacity of 112 mA h g^{-1} at 0.1 C with 0.82 retention (at 1.0 C) after 500 cycles.[23] Despite obtaining such a good capacity using autoclave for coating, makes this method less cost efficient.

In this study, we utilized a feasible cost-efficient method to fabricate a $LiFePO_4$ coated CFs cathode electrode for a composite structural battery. To the best of our knowledge, this approach has not been reported elsewhere. The CFs tow performs not only as current collector, but also provides mechanical stiffness and strength. The choice of $LiFePO_4$ as the cathode material is based not only on its non-toxic properties, but also on its cost-effectiveness when compared to other cathode materials. This makes it highly beneficial for scale-up applications. $LiFePO_4$ cathode slurry are composed of $LiFePO_4$ particles, carbon black particles and PVDF to bind the particles. To seek an optimum $LiFePO_4$ slurry ratio, different ratios of $LiFePO_4$ were prepared. The morphology and properties of $LiFePO_4$ coatings on CFs tow were investigated. Electrochemical analysis was conducted to evaluate capacity, rate performance and cycling life. Furthermore, tensile testing for the structural cathode was carried out to investigate not only mechanical strength, but also the crack propagation of $LiFePO_4$ coating on the surface of CFs.

Experimental

Materials

$LiFePO_4$ (LFP) whose particle size ranging between 100 and 300 nm was supplied by TARGRAY. Carbon black (CB, SUPER C65) with dimension of 20 nm was purchased from TIMCAL. Anhydrous 1-methyl-2-pyrrolidinone (NMP, purity of 99.5%) and polyvinylidene fluoride (PVDF) with molecular weight 534 000 measured by GPC were purchased from Sigma Aldrich. Furthermore, lithium hexafluorophosphate solution in ethylene carbonate and dimethyl carbonate (1.0 M $LiPF_6$ in EC/DEC = 50/50, battery grade) electrolyte were also obtained from Sigma-Aldrich. All purchased chemicals were utilised without any pre purifications. Unidirectional (UD) T300 CF tow (A38-6k) were obtained from DowAksa (Turkey).

Fabrication of UD carbon fibre substrate

To prepare a CFs substrate, UD CFs tow (6k) was placed onto a Si rubber plate with dimensions of 75 mm × 25 mm. Subsequently, the tow was secured with tape. Next, the CFs were wrapped with a release film layer, peel-ply strip, and breather on a 30 × 30 cm stainless-steel plate. Afterward, the PVDF binder, consisting of 0.2 g of PVDF dissolved in 1 mL of NMP, was used for vacuum infusion. The prepared mold was then placed in a hot press for the coating step at 80 °C with an applied pressure of approximately 3 bar for 30 minutes. This process was carried out in a vacuum environment.

Fabrication of $LiFePO_4$/CF structural cathode

Developed UD carbon fibres substrate was used to fabricate the $LiFePO_4$/CF structural cathode for this study. To fabricate $LiFePO_4$ slurry for the CFs structural cathode, different ratios of $LiFePO_4$, carbon black, NMP and PVDF as listed in Table 1 were prepared.

The composed cathode materials were poured into a mixed solvent (0.48 mL of NMP + 2 mL of acetone) and stirred using a magnet stirrer at 40 °C for 30 min. Then, the product was sonicated for the same temperature and duration in a bath sonicator and stirred for further 30 min at 40 °C prior to coating onto the CFs substrate. The cathode slurry was applied to a stainless-steel plate using a doctor blade with a thickness of 200 μm. Next, a CFs substrate, which was attached to a Si rubber plate, was placed on top of the electrode slurry. The same vacuum bagging procedure used to prepare the CFs substrate was then conducted. The vacuum-sealed mold was transferred to a hot press and kept at 120 °C for 2 hours under 1 bar pressure, as shown in Scheme 1.

Characterization methods

X-ray diffraction (XRD). X-ray diffraction (XRD) was performed using a Malvern PANalytical X-pert powder with Cu Kα radiation operating at 30 mA and 40 kV. The measurement was over the range of diffraction angle 2θ = 10–60°, with a scan speed of 3.3° min^{-1} at room temperature.

Raman spectroscopy. Raman results were obtained using InVia confocal Raman spectroscopy (REINSHAW, UK), equipped with a 758 nm laser. Raman results were used to study the DG band changes between pristine CFs tow and series of $LiFePO_4$/CF.

Morphology of structural battery electrolyte. Morphology of structural battery electrolyte was examined using scanning electron microscopy (SEM) technique using SEM (Supra 55VP, ZEISS). Before measurements, all samples were vacuum dried in a conventional oven to perfectly remove moisture prior to conducting SEM. The dried $LiFePO_4$/CF samples were coated with 3 nm gold. SEM imaging of surface and cross-section of the samples with different magnifications was conducted. EDX

Table 1 $LiFePO_4$ slurry ratio for structural cathode

$LiFePO_4$ (wt%)	Carbon black (wt%)	PVDF (wt%)	NMP
92	2	6	1 : 4 ratio (PVDF : NMP) in 2 mL of acetone
90	4	6	
88	4	8	
78	10	12	

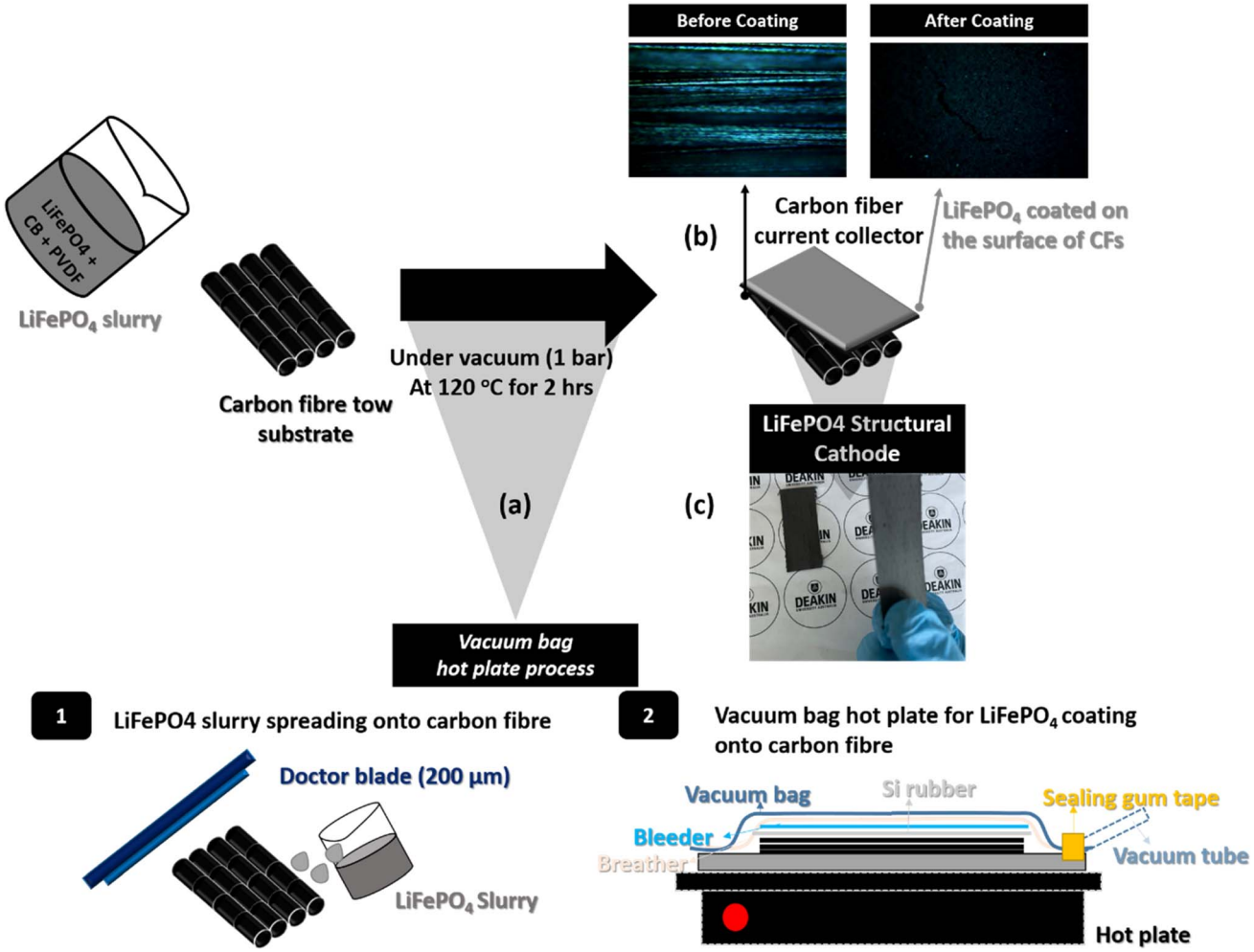

Scheme 1 A schematic of $LiFePO_4$/CF production; (a) the fabrication details of a vacuum bag hot plate process for $LiFePO_4$ slurry coating onto CFs tow (b) optical images (surface) before/after $LiFePO_4$ coating onto UD CFs substrate and (c) an image of the $LiFePO_4$/CF structural cathode.

measurements were also carried out to obtain the elemental mapping of samples. The operating voltage of 20 kV was set for EDX.

For electrochemical cycling experiments for half cell ($LiFePO_4$/CF-Li). For electrochemical cycling experiments for half cell ($LiFePO_4$/CF-Li), a 3023 coin-cell was used. The half-cell was assembled with a structural cathode ($LiFePO_4$/CF), lithium foil, 250 µm thickness glass microfibre filter, and 1 M $LiPF_6$ (EC : DEC of 1 : 1) as working electrode, reference electrode, separator, and electrolyte. All coin-cell fabrication was conducted in a glove box with argon environment (<1 ppm O_2 and H_2O), and $LiFePO_4$/CF was vacuum dried in a conventional oven for 24 h at 60 °C for 24 before the cell fabrication step.

According to standard test method D3039, characterization of mechanical performance of the $LiFePO_4$/CF electrode. According to standard test method D3039, characterization of mechanical performance of the $LiFePO_4$/CF electrode were carried out with the rate of 0.5 mm min^{-1} to study the elastic potential as well as surface crack propagation of the $LiFePO_4$/CF electrode using a universal machine testing (UTM, Instron 5967, UK equipped with load cell of 1 kN).

Results and discussions

1. Structural characterization of the $LiFePO_4$/CF electrode composite

Scheme 1 shows the entire process of the $LiFePO_4$ cathode coating on to UD CFs substrate using a facile vacuum compression molding press. In Fig. 1, the microstructure of 78 $LiFePO_4$/CF electrode composite was investigated *via* SEM. As illustrated in Fig. 1(a) and (b), $LiFePO_4$ slurry was adequately adhered onto the surface of pre-prepared CFs tow substrate. Furthermore, the thickness of 78 $LiFePO_4$/CF is confirmed as 42.9 µm *via* the cross-section image in Fig. 1(b) which is comparable to the commercial electrodes having 20–30 µm thickness. Fig. 1(c) shows the $LiFePO_4$ coating onto the surface of CFs at low magnification which is uniform.

Fig. 1(d) reveals the distribution of coated particles ($LiFePO_4$ and carbon black) on the surface of CFs, demonstrating a good particle distribution on the coating surface. In addition, the particle distribution on the surface of $LiFePO_4$ coated CFs was evaluated *via* EDX (Fig. S2†) as it enables identifications of key

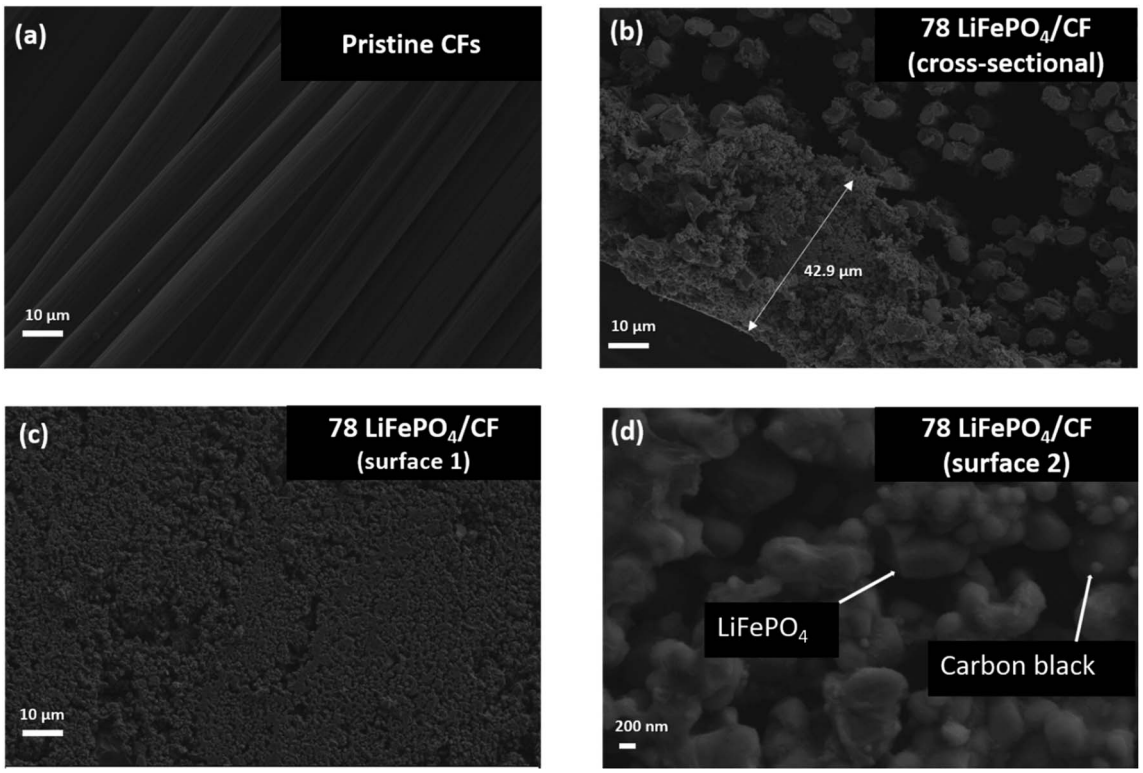

Fig. 1 Morphology investigation *via* SEM; (a) CF tow pristine, (b) the cross-sectional image of 78 $LiFePO_4$ onto CFs (78 $LiFePO_4$/CF) to investigate the coating quality (c) and (d) surface investigation with low and high magnification.

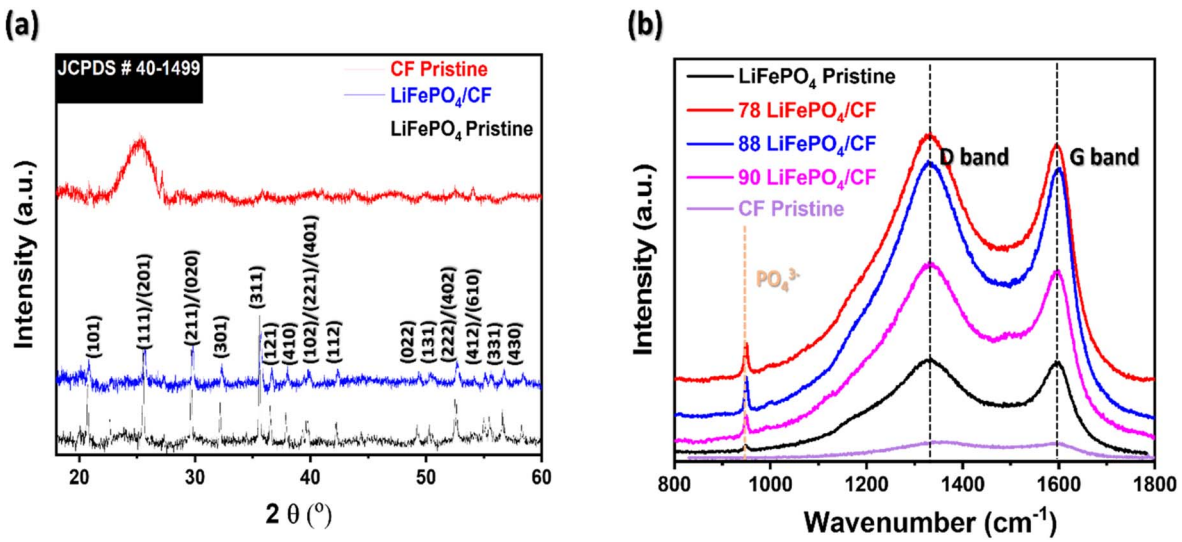

Fig. 2 Microstructural evaluation of neat materials (CFs pristine and $LiFePO_4$ powder) and different $LiFePO_4$ slurry applied structural cathode composite *via* (a) XRD and (b) Raman.

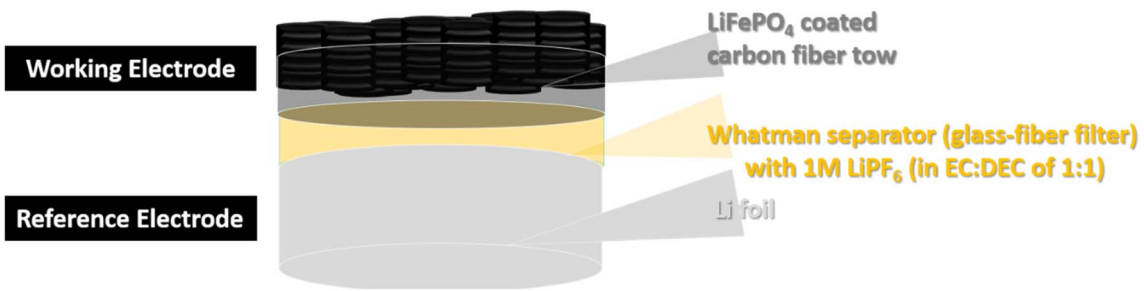

Fig. 3 Schematic Illustration of the coin cell design as a half-cell *vs.* Li/Li^+.

elements (Fe and P from $LiFePO_4$, F from PVDF) distribution and no distinct defects was found.

Fig. 2(a) shows XRD graphs of $LiFePO_4$ and $LiFePO_4$/CF. All evaluated diffraction peaks can be indexed to crystalline orthorhombic $LiFePO_4$ phase according to JCPDS card no. is 40–1499.[25,26] In Fig. 2(a), the CFs peak disappeared from the XRD pattern of $LiFePO_4$/CF electrode composite, indicating that $LiFePO_4$ is coated on to the surface of CFs substrate. Furthermore, by comparing the XRD pattern between the electrode composite and $LiFePO_4$, no significant peaks were found in the $LiFePO_4$/CF composite, revealing that vacuum compression moulding approach did not influence the $LiFePO_4$ crystalline structure.

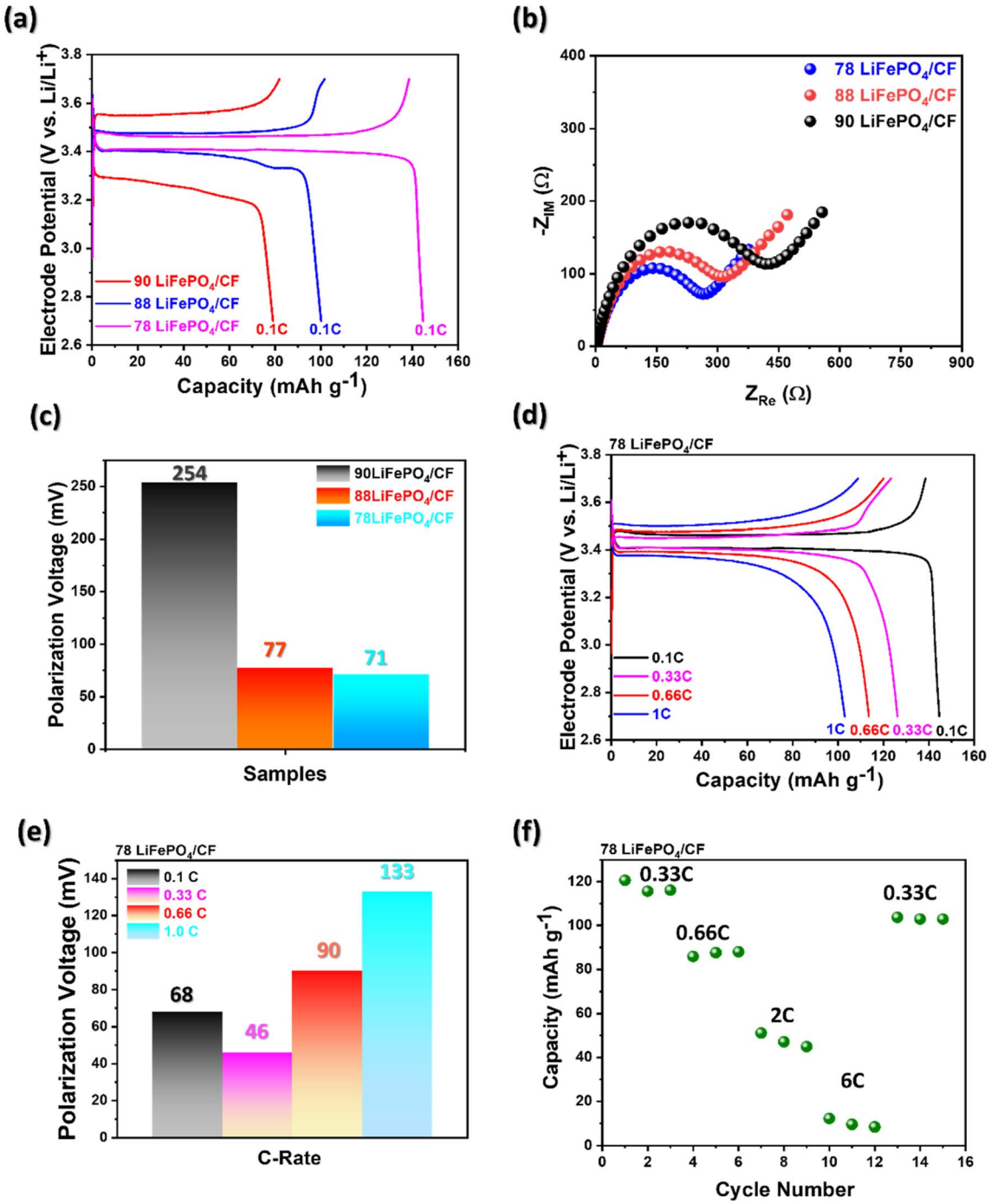

Fig. 4 Electrochemical examination of the $LiFePO_4$/CF electrode samples with 1.0 M $LiPF_6$, ethylene carbonate (EC) : diethyl carbonate (DEC) (1 : 1 by weight) as electrolyte; (a) charge–discharge profile with different $LiFePO_4$ slurry applied structural cathode, (b) electrochemical impedance spectroscopy (EIS) of different LiFePO4 slurry samples, (c) polarization voltage in different LFP slurry composition at 0.1 C (d) charge–discharge profile of 78$LiFePO_4$/CF at different *C*-rate, (e) polarization voltage changes at 78 $LiFePO_4$/CF in different *C*-rate (0.1/0.33/0.66/1.0 C) and (f) Specific capacities of 78$LiFePO_4$/CF at different *C*-rates.

Table 2 Different LFP slurry composition series and their 2 relative values of R_s and R_{ct} based on the Nyquist Plots in Fig. 4(b)

	Weight of LFP (mg cm^{-2})	R_s (Ω cm^{-1})	R_{ct} (Ω)
78 $LiFePO_4$/CF	7.53	3.19	263.6
88 $LiFePO_4$/CF	5.78	2.99	313.6
90 $LiFePO_4$/CF	4.94	2.84	417.1

In Fig. 2(b), two distinct peaks were appeared at 1335 cm^{-1} and 1596 cm^{-1} which is related to D-band (sp^3 hybridization, disordered carbon) and G-band (sp^2 hybridization, graphite), correspondingly.[27,28] Xie *et al.* reported that the intensity ratio of I_D/I_G is an index of the degree of disorder carbon layers.[29] The I_D/I_G ratio of 78 $LiFePO_4$/CF is 1.01 which is lower in comparison with 88 $LiFePO_4$/CF (1.03) and 90 $LiFePO_4$/CF (1.05). This suggests that 78 $LiFePO_4$/CF has graphite-like coating layers compared to other composite samples which present more amorphous coating layers, thereby it may influence the lithium-ion interaction while performing electrochemical analysis.

Shi *et al.* reported the peak between 500 and 1100 cm^{-1} in Raman spectra can be associated with vibration of the Fe–O and PO_4^{3-} group.[29] As shown in Fig. 2(b), all $LiFePO_4$ coated CFs composite displayed PO_4^{3-} peak at 950 cm^{-1}, and hence these are another evidence of $LiFePO_4$ coating performance on the surface of CFs which is in agreement with XRD result.

2. The half-cell performance

For the half-cell performance of the $LiFePO_4$ composite electrodes, the half-cell was fabricated as depicted on Fig. 3.

As illustrated in Fig. 4(a), the results of electrochemical performance of the fabricated cathode at 0.1 C exhibit that the different $LiFePO_4$ electrode slurry ratios influenced the capacity difference. The electrochemical performance at 0.1 C reveals that 78 $LiFePO_4$/CF indicated the highest capacity as 144 mA h g^{-1} compared to the other ratio samples. As mentioned earlier about the $LiFePO_4$ coating performance in regards with I_D/I_G ratio, this result may be obtained by more graphitized coating structure, which enables better lithium-ion intercalation, on 78 $LiFePO_4$/CF compared to other samples. Sanchez *et al.* reported that the lower overall resistance between electrolyte and electrode attaining from electrochemical impedance spectroscopy (EIS) can be reflected to superior capacity performance.[29] In addition, Ferg and Vuuren reported a battery cell having higher internal resistance (R_{ct}) could not perform well compared to a cell with lower R_{ct}.[30]

As shown in Fig. 4(b) and Table 2, the resistance between electrolyte and electrode for 78 $LiFePO_4$/CF, 88 $LiFePO_4$/CF and 90 $LiFePO_4$/CF samples were obtained *via* the intercept on the real axis (Z_{re}) in the intrinsic resistance (R_s) of the spectra to be 3.19, 2.99 and 2.84 Ω cm^{-1}, respectively. In addition, the semicircle between high and low frequencies indicates the R_{ct}

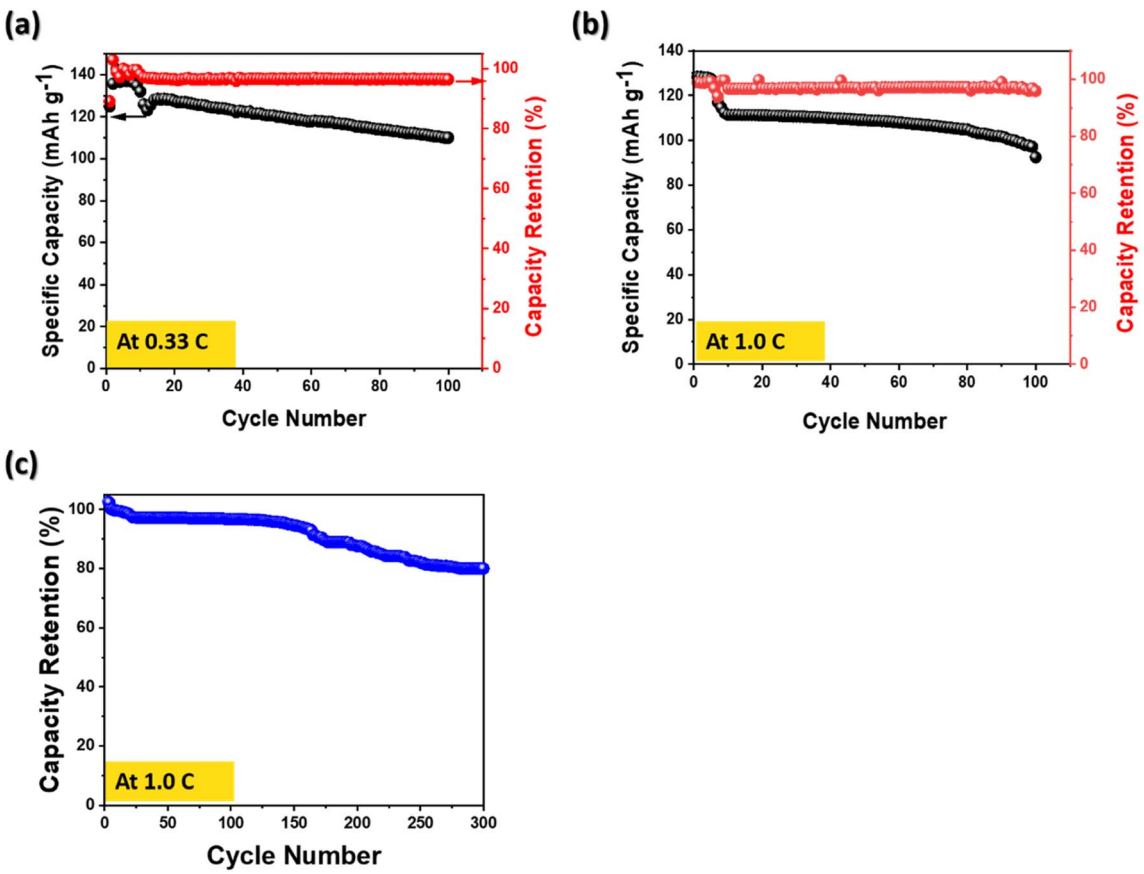

Fig. 5 Long-term cycling stability for 78 $LiFePO_4$/CF composite electrode (a) at 0.33 *C*-rate over 100 cycle (b) at 1.0 *C*-rate over 100 cycle and (c) coulombic efficiency at 1.0 *C*-rate over 300 cycle.

Table 3 Performance comparison of the $LiFePO_4$ composite electrode for structural batteries with previous studies

	Method	Carbon fibre	Materials	Capacity (mA h g^{-1})	Cycling retention (%)	Mass loading (mg cm^{-2})	Ref.
1	Hot press (at 120 °C under 1 bar pressure)	6k tow	$LiFePO_4$/carbon black/PVDF	144 (at 0.1 C)	96.4 at 0.33 C, 95.8 at 1.0 C (100 cycles) and 81.2 at 1.0 C (300 cycles)	4.7	This work
2	Electro-deposition (EPD)	12k tow	$LiFePO_4$/carbon black/PVDF Acetone and surfactant for EPD	110 (at 0.1 C)	62 at 1.0 C (500 cycles)	n/a	11
3	Electro-deposition (EPD)	12k tow	$LiFePO_4$/carbon black/graphene oxide (GO) DMF and surfactant for EPD	131 (at 0.1 C)	91 at 1.0 C (500 cycles)	1	39
4	Electro-deposition (EPD)	Carbon cloth	$LiFePO_4$/carbon black EtOH	110 (at 0.1 C)	80 at 0.5 C (300 cycles)	20	24
5	Electro-deposition (EPD)	Carbon cloth	$LiFePO_4$/carbon black EtOH	140 (at 0.1 C)	84 at 0.1 C (100 cycles)	10	24
6	Autoclave	Woven fabric	$LiFePO_4$/carbon black/PVDF	112 (at 0.1 C)	82 at 1.0 C(500 cycles)	n/a	23

and it was the smallest in 78$LiFePO_4$/CF (263.6 Ω) compared to 88$LiFePO_4$/CF (313.6 Ω) and 90$LiFePO_4$/CF (417.1 Ω). According to obtained resistances, the interfacial redox reaction is more likely to be favoured in 78$LiFePO_4$/CF compared to other samples.

Cui *et al.* reported that cycle stability can be enhanced by reducing interfacial resistance between the electrolyte and electrode, as well as decreasing polarization voltage during charging and discharging.[31] Additionally, Wang *et al.* found that an increase in cell polarization leads to capacity fading.[32] Fig. 4(c) shows the lowest polarization voltage at 78 LiFePO4/CF compared to other slurry composition samples, and it also exhibits the smallest Rct value as mentioned earlier. These results explain the capacity fading observed in different slurry compositions in terms of electrochemical performance at 0.1 C, as shown in Fig. 4(a), by correlating it with interfacial resistance and polarization voltage.

Fig. 4(d) shows charge/discharge profiles at different *C*-rates for a CFs electrode coated *via* a vacuum hot press with the slurry composition 78 : 10 : 2 ($LiFePO_4$: PVDF : CB). The voltage plateau of 78 $LiFePO_4$/CF was indicated as around 3.4 V *vs.* Li^+/Li, attributed to the redox reaction of Fe^{2+}/Fe^{3+} in agreement of the previous studies.[33,34] Furthermore, the specific capacity is decreasing *via* increasing *C*-rate from 0.1 C to 1.0 C in agreement with the previous reported.[35,36] Interestingly, Fig. 4(e) shows increasing trend in polarization voltage by increasing *C*-rate, and hence it could be evaluated as a crucial parameter on battery performance.

As shown in Fig. 4(f), the performance of 78$LiFePO_4$/CF reduces with enhancing *C*-rate. Nevertheless, it is reversible procedure because the initial capacity was returned by returning to 0.33 C.

Fig. 5(a–c) show a long-term cycling stability which is a key parameter for an electrode of Li-ion batteries. Two different conditions for long-term cycling stability were conducted not only at 0.33 C over 100 cycles, but also 1.0 C over 300 cycles. Fig. 5(a) and (b) exhibit slightly fading the specific capacity at 0.33 C and at 1.0 C over 100 cycles. However, no significant capacity drop was observed and also high-capacity retentions of 96.4% at 0.33 C and 95.8% at 1.0 C were obtained. Previous works have reported that the capacity fade occurred by growth of the negative electrode SEI, consequently it causes a continuous capacity fading.[37,38]

In addition, the capacity over 300 cycles exhibited 81.2% retention, demonstrating that the performance degradation was not occurred rapidly at a high *C*-rate. By comparing the obtained electrochemical performance with the previous studies in Table 3, the structural cathode prepared *via* a vacuum bag hot plate process reveals a potential to utilize for structural batteries.

3. Mechanical properties of structural cathode

The tensile tests were carried out to study mechanical properties of structural CFs cathodic composite as well as investigate propagating crack regions while applying force. Fig. 5 exhibits the results of tensile test and photography of $LiFePO_4$ coating crack propagation on the surface of CFs. The first surface crack was initiated in the region 1 in Fig. 6(a) and confirmed through a photography of the region 1 in Fig. 6(c). According to Fig. 6(a) and (b), the surface crack propagation was continued until the fracture region appeared in the stress–strain curve. In addition, the crack propagation occurred at the outer surface area of the composite electrode. However, the resultants of 90 $LiFePO_4$/CF in Fig. 6(b and d) showed a significant surface crack propagation at the centre and outer surface area compared to 78 $LiFePO_4$/CF. Interestingly after the test, 78 $LiFePO_4$/CF sustained its structure as well as $LiFePO_4$ coating on the surface of CFs compared to 90 $LiFePO_4$/CF. This phenomenon may be attributed by the different ratio of PVDF in the cathode slurry. Because it influences determining the degree of binding $LiFePO_4$ and CB particles on the surface of CFs.[38–40]

Furthermore, the optimized structural cathode composite (78 $LiFePO_4$/CF) in Table 4 shows high mechanical performances, 538.7 MPa tensile strength, 4.30 GPa elastic modulus and 64.4 MJ m^{-3} toughness. This result indicates that higher binder affects not only effectively holding active materials, but also physically bonding to CFs substrate.[41,42] According to these

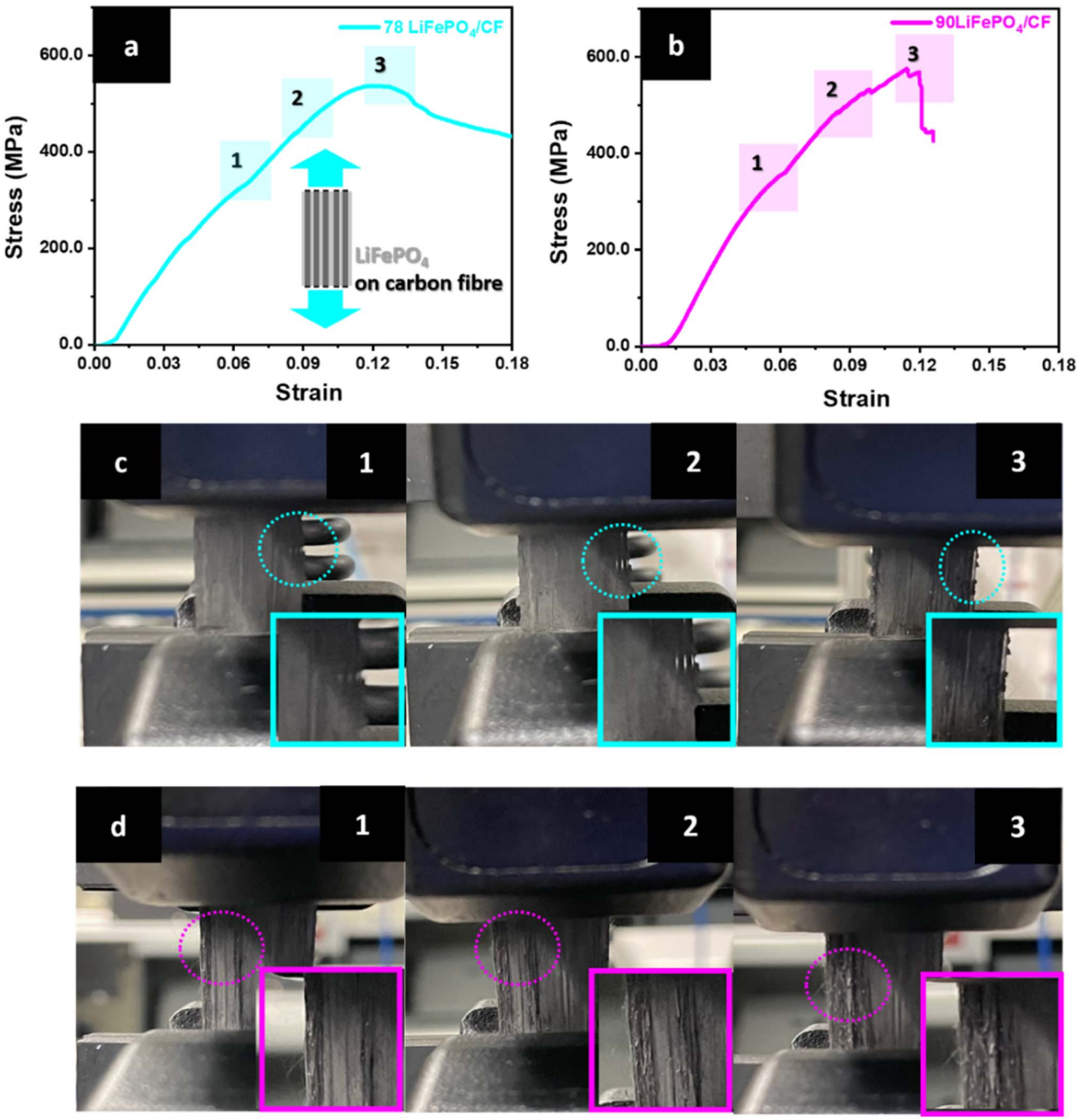

Fig. 6 Tensile testing result of the 78$LiFePO_4$/CF and 90$LiFePO_4$/CF composite electrode (a and b) stress–strain curve for the composite electrodes and (c and d) $LiFePO_4$ (LFP) coating crack propagation for the composite electrodes while testing.

Table 4 Mechanical properties of the CFs composites coated with different ratio of $LiFePO_4$[a]

Sample	Young's modulus (GPa)	Stress at elongation at break (MPa)	Toughness (MJ m^{-3})
78 $LiFePO_4$	4.30 ± 0.23	538.7 ± 0.99	64.4 ± 0.14
90 $LiFePO_4$	4.74 ± 1.06	517.9 ± 79.27	42.5 ± 5.09

[a] Toughness was calculated by integrating the tensile stress–strain curve.

results, a vacuum bag hot press process to coat $LiFePO_4$ on CFs is a potential applicable method for a structural composite battery.

Conclusions

In summary, we employed a straightforward approach to fabricate a $LiFePO_4$-coated CFs composite electrode for structural batteries. Based on XRD and Raman analyses, the $LiFePO_4$ slurry was well-coated onto the surface of CFs. Furthermore, the 78 $LiFePO_4$/CF composite exhibited thicker graphite coating layers compared to other samples, as evidenced by the ratio of I_D/I_G, which also confirmed its influence on electrochemical performance. The morphology of the $LiFePO_4$ coating on the CFs' surface, as observed *via* SEM, displayed not only flawless surface coating but also clear separation between the $LiFePO_4$ coating layer and CFs in the cross-sectional view.

The optimized cathode composite half-cell, with high mechanical performance (538.7 MPa tensile strength and 4.12 GPa elastic modulus), achieved a discharge capacity of 144 mA h g^{-1} at 0.1 C and 102 mA h g^{-1} at 1.0 C. Additionally, long-term cycling stability demonstrated 96.4% (over 100 cycles) and 81.2% (over 300 cycles) at 0.33 C and 1.0 C, respectively. These results suggest that the developed $LiFePO_4$-coated CFs composite electrode holds great promise as a candidate for cathode materials in structural battery development.

Conflicts of interest

There are no conflicts to declare.

Acknowledgements

The authors gratefully acknowledge the Australian Research Council (ARC) Research Hub for Future Fibres (IH140100018) funded by the Australian Government for their financial support.

References

1 S. Solaymani, CO_2 emissions patterns in 7 top carbon emitter economies: The case of transport sector, *Energy*, 2019, **168**, 989–1001, DOI: 10.1016/j.energy.2018.11.145.
2 M. Pichler, N. Krenmayr, E. Schneider and U. Brand, EU industrial policy: Between modernization and transformation of the automotive industry, *Environ. Innov. Soc. Transit.*, 2021, **38**, 140–152, DOI: 10.1016/j.eist.2020.12.002.
3 C. C. Kwasi-Effah and T. Rabczuk, Dimensional analysis and modelling of energy density of lithium-ion battery, *J. Energy Storage*, 2018, **18**, 308–315, DOI: 10.1016/j.est.2018.05.002.
4 X. Lv, W. Wei, B. Huang and Y. Dai, Achieving high energy density for lithium-ion battery anodes by Si/C nanostructure design, *J. Mater. Chem. A*, 2019, **7**, 2165–2171, DOI: 10.1039/C8TA10936B.
5 X. Dong, L. Chen, X. Su, Y. Wang and Y. Xia, Flexible Aqueous Lithium-Ion Battery with High Safety and Large Volumetric Energy Density, *Angew. Chem., Int. Ed.*, 2016, **55**, 7474–7477, DOI: 10.1002/anie.201602766.
6 A. Jacob, Carbon fibre and cars – 2013 in review, *Reinf. Plast.*, 2014, **58**, 18–19, DOI: 10.1016/S0034-3617(14)70036-0.
7 H. Adam, Carbon fibre in automotive applications, *Mater. Des.*, 1997, **18**, 349–355, DOI: 10.1016/S0261-3069(97)00076-9.
8 K. Badii, J. S. Church, G. Golkarnarenji, M. Naebe and H. Khayyam, Chemical structure based prediction of PAN and oxidized PAN fiber density through a non-linear mathematical model, *Polym. Degrad. Stab.*, 2016, **131**, 53–61, DOI: 10.1016/j.polymdegradstab.2016.06.019.
9 W. Kang, N. Deng, J. Ju, Q. Li, D. Wu, X. Ma, *et al.*, A review of recent developments in rechargeable lithium–sulfur batteries, *Nanoscale*, 2016, **8**, 16541–16588, DOI: 10.1039/C6NR04923K.
10 V. Ghanooni Ahmadabadi, K. Shirvanimoghaddam, R. Kerr, N. Showkath and M. Naebe, Structure-rate performance relationship in Si nanoparticles-carbon nanofiber composite as flexible anode for lithium-ion batteries, *Electrochim. Acta*, 2020, **330**, 135232, DOI: 10.1016/j.electacta.2019.135232.
11 J. Hagberg, H. A. Maples, K. S. P. Alvim, J. Xu, W. Johannisson, A. Bismarck, *et al.*, Lithium iron phosphate coated carbon fiber electrodes for structural lithium ion batteries, *Compos. Sci. Technol.*, 2018, **162**, 235–243, DOI: 10.1016/j.compscitech.2018.04.041.
12 H. Khayyam, R. N. Jazar, S. Nunna, G. Golkarnarenji, K. Badii, S. M. Fakhrhoseini, *et al.*, PAN precursor fabrication, applications and thermal stabilization process in carbon fiber production: Experimental and mathematical modelling, *Prog. Mater. Sci.*, 2020, **107**, 100575, DOI: 10.1016/j.pmatsci.2019.100575.
13 L. E. Asp and E. S. Greenhalgh, Structural power composites, *Compos. Sci. Technol.*, 2014, **101**, 41–61, DOI: 10.1016/j.compscitech.2014.06.020.
14 J. Galos, K. Pattarakunnan, A. S. Best, I. L. Kyratzis, C.-H. Wang and A. P. Mouritz, Energy Storage Structural Composites with Integrated Lithium-Ion Batteries: A Review, *Adv. Mater. Technol.*, 2021, **6**, 2001059, DOI: 10.1002/admt.202001059.
15 J. Choi, O. Zabihi, R. J. Varley, B. Fox and M. Naebe, Enhancement of ionic conduction and mechanical properties for all-solid-state polymer electrolyte systems through ionic and physical bonding, *Mater. Today Chem.*, 2022, **23**, 100663, DOI: 10.1016/j.mtchem.2021.100663.
16 J. Choi, O. Zabihi, R. J. Varley, B. Fox and M. Naebe, High Performance Carbon Fiber Structural Batteries Using Cellulose Nanocrystal Reinforced Polymer Electrolyte, *ACS Appl. Mater. Interfaces*, 2022, **14**, 45320–45332, DOI: 10.1021/acsami.2c11034.
17 J. Choi, O. Zabihi, R. Varley, J. Zhang, B. L. Fox and M. Naebe, Multiple Hydrogen Bond Channel Structural Electrolyte for an Enhanced Carbon Fiber Composite Battery, *ACS Appl. Energy Mater.*, 2022, **5**, 2054–2066, DOI: 10.1021/acsaem.1c03354.

18 Y. Yu, B. Zhang, M. Feng, G. Qi, F. Tian, Q. Feng, *et al.*, Multifunctional structural lithium ion batteries based on carbon fiber reinforced plastic composites, *Compos. Sci. Technol.*, 2017, **147**, 62–70, DOI: **10.1016/j.compscitech.2017.04.031**.

19 P. Liu, E. Sherman and A. Jacobsen, Design and fabrication of multifunctional structural batteries, *J. Power Sources*, 2009, **189**, 646–650, DOI: **10.1016/j.jpowsour.2008.09.082**.

20 I. J. Davidson, R. S. McMillan, J. J. Murray and J. E. Greedan, Lithium-ion cell based on orthorhombic $LiMnO_2$, *J. Power Sources*, 1995, **54**, 232–235, DOI: **10.1016/0378-7753(94)02074-D**.

21 J.-M. Chen, C.-H. Hsu, Y.-R. Lin, M.-H. Hsiao and G. T.-K. Fey, High-power $LiFePO_4$ cathode materials with a continuous nano carbon network for lithium-ion batteries, *J. Power Sources*, 2008, **184**, 498–502, DOI: **10.1016/j.jpowsour.2008.04.022**.

22 J. Ying, C. Jiang and C. Wan, Preparation and characterization of high-density spherical $LiCoO_2$ cathode material for lithium ion batteries, *J. Power Sources*, 2004, **129**, 264–269, DOI: **10.1016/j.jpowsour.2003.10.007**.

23 H.-W. Park, M.-S. Jang, J.-S. Choi, J. Pyo and C.-G. Kim, Characteristics of woven carbon fabric current collector electrodes for structural battery, *Compos. Struct.*, 2021, **256**, 112999, DOI: **10.1016/j.compstruct.2020.112999**.

24 K. Moyer, R. Carter, T. Hanken, A. Douglas, L. Oakes and C. L. Pint, Electrophoretic deposition of $LiFePO_4$ onto 3-D current collectors for high areal loading battery cathodes, *Mater. Sci. Eng. B*, 2019, **241**, 42–47, DOI: **10.1016/j.mseb.2019.02.003**.

25 W. Li, A. Garg, M. L. P. Le, C. Ruhatiya, L. Gao and V. M. Tran, Electrochemical performance investigation of $LiFePO_4$/C0.15−x (x = 0.05, 0.1, 0.15 CNTs) electrodes at various calcination temperatures: Experimental and Intelligent Modelling approach, *Electrochim. Acta*, 2020, **330**, 135314, DOI: **10.1016/j.electacta.2019.135314**.

26 B. Wang, Q. Wang, B. Xu, T. Liu, D. Wang and G. Zhao, The synergy effect on Li storage of $LiFePO_4$ with activated carbon modifications, *RSC Adv.*, 2013, **3**, 20024–20033, DOI: **10.1039/C3RA44218G**.

27 A. Manthiram, A. Vadivel Murugan, A. Sarkar and T. Muraliganth, Nanostructured electrode materials for electrochemical energy storage and conversion, *Energy Environ. Sci.*, 2008, **1**, 621–638, DOI: **10.1039/B811802G**.

28 X. Liu, X. Liu, B. Sun, H. Zhou, A. Fu, Y. Wang, *et al.*, Carbon materials with hierarchical porosity: Effect of template removal strategy and study on their electrochemical properties, *Carbon*, 2018, **130**, 680–691, DOI: **10.1016/j.carbon.2018.01.046**.

29 Y. Xie, F. Song, C. Xia and H. Du, Preparation of carbon-coated lithium iron phosphate/titanium nitride for a lithium-ion supercapacitor, *New J. Chem.*, 2015, **39**, 604–613, DOI: **10.1039/C4NJ01169D**.

30 E. E. Ferg and F. van Vuuren, Comparative capacity performance and electrochemical impedance spectroscopy of commercial AA alkaline primary cells, *Electrochim. Acta*, 2014, **128**, 203–209, DOI: **10.1016/j.electacta.2013.08.110**.

31 Z. Cui, S. Inoue, J. Hassoun and Y. Tominaga, Enhanced Performance of All-Solid-State Li Metal Battery Based on Polyether Electrolytes with $LiNO_3$ Additive, *Macromol. Chem. Phys.*, 2022, **223**, 2100396, DOI: **10.1002/macp.202100396**.

32 F. Wang, Z. Lin, L. Liu, X. Wei, S. Lin, L. Dai, *et al.*, Does Polarization Increase Lead to Capacity Fade?, *J. Electrochem. Soc.*, 2020, **167**, 090549, DOI: **10.1149/1945-7111/ab956b**.

33 X. Rui, X. Zhao, Z. Lu, H. Tan, D. Sim, H. H. Hng, *et al.*, Olivine-Type Nanosheets for Lithium Ion Battery Cathodes, *ACS Nano*, 2013, **7**, 5637–5646, DOI: **10.1021/nn4022263**.

34 V. A. Sugiawati, F. Vacandio, C. Perrin-Pellegrino, A. Galeyeva, A. P. Kurbatov and T. Djenizian, Sputtered Porous Li-Fe-P-O Film Cathodes Prepared by Radio Frequency Sputtering for Li-ion Microbatteries, *Sci. Rep.*, 2019, **9**, 11172, DOI: **10.1038/s41598-019-47464-2**.

35 A. Tomaszewska, Z. Chu, X. Feng, S. O'Kane, X. Liu, J. Chen, *et al.*, Lithium-ion battery fast charging: A review, *ETransportation*, 2019, **1**, 100011, DOI: **10.1016/j.etran.2019.100011**.

36 G. Ning, B. Haran and B. N. Popov, Capacity fade study of lithium-ion batteries cycled at high discharge rates, *J. Power Sources*, 2003, **117**, 160–169, DOI: **10.1016/S0378-7753(03)00029-6**.

37 M. Safari and C. Delacourt, Aging of a Commercial Graphite/$LiFePO_4$ Cell, *J. Electrochem. Soc.*, 2011, **158**, A1123, DOI: **10.1149/1.3614529**.

38 A. J. Smith, J. C. Burns, X. Zhao, D. Xiong and J. R. Dahn, A High Precision Coulometry Study of the SEI Growth in Li/Graphite Cells, *J. Electrochem. Soc.*, 2011, **158**, A447, DOI: **10.1149/1.3557892**.

39 J. S. Sanchez, J. Xu, Z. Xia, J. Sun, L. E. Asp and V. Palermo, Electrophoretic coating of $LiFePO_4$/Graphene oxide on carbon fibers as cathode electrodes for structural lithium ion batteries, *Compos. Sci. Technol.*, 2021, **208**, 108768, DOI: **10.1016/j.compscitech.2021.108768**.

40 X.-M. Fan, Y.-D. Huang, H.-X. Wei, L.-B. Tang, Z.-J. He, C. Yan, J. Mao, K.-H. Dai and J.-C. Zheng, Surface Modification Engineering Enabling 4.6 V Single-Crystalline Ni-Rich Cathode with Superior Long-Term Cyclability, *Adv. Funct. Mater.*, 2022, **32**(6), 2109421, DOI: **10.1002/adfm.202109421**.

41 Y.-D. Huang, H.-X. Wei, P.-Y. Li, Y.-H. Luo, Q. Wen, D.-H. Le, Z.-J. He, H.-Y. Wang, Y.-G. Tang, C. Yan, J. Mao, K.-H. Dai, X.-H. Zhang and J.-C. Zheng, Enhancing structure and cycling stability of Ni-rich layered oxide cathodes at elevated temperatures via dual-function surface modification, *J. Energy Chem.*, 2022, **75**, 301–309, DOI: **10.1016/j.jechem.2022.08.010**.

42 Y.-d Huang, H.-X. Wei, P.-Y. Li, L.-B. Tang, Y.-H. Luo, X.-M. Fan, C. Yan, J. Mao, K.-H. Dai, H.-Z. Chen, X.-h Zhang and J.-c Zheng, Rational design of surface reconstruction with pinning effect to relieving bulk fatigue for high energy single-crystal Ni-rich cathodes, *J. Chem. Eng.*, 2023, **470**, 144254, DOI: **10.1016/j.cej.2023.144254**.